Bimetallic Phosphide (Ni,Cu) 2 P Nanoparticles by Inward Phosphorus Migration and Outward Copper Migration

Anh-Minh Nguyen, Mounib Bahri, Sébastien Dreyfuss, Simona Moldovan, Antoine Miche, Christophe Méthivier, Ovidiu Ersen, Nicolas Mézailles, Sophie Carenco

Bimetallic Phosphide $(Ni,Cu)_2P$ Nanoparticles by Inward Phosphorus Migration and Outward Copper Migration

Anh-Minh Nguyen,[1] Mounib Bahri,[3] Sébastien Dreyfuss,[2] Simona Moldovan,[3] Antoine Miche,[4] Christophe Méthivier,[4] Ovidiu Ersen,[3] Nicolas Mézailles,[2,*] Sophie Carenco[1,*]

[1] *Sorbonne Université, CNRS, Collège de France, Laboratoire de Chimie de la Matière Condensée de Paris, 4 place Jussieu, 75005 Paris, France*

[2] *Laboratoire Hétérochimie Fondamentale et Appliquée, CNRS, Université Paul Sabatier, 118 Route de Narbonne, 31062 Toulouse, France*

[3] *Institut de Physique et de Chimie des Matériaux de Strasbourg (IPCMS), UMR 7504 CNRS - Université de Strasbourg 23, rue du Loess BP 43, F-67034 Strasbourg, France*

[4] *Sorbonne Université, CNRS, Laboratoire de Réactivité de Surface, 4 place Jussieu, 75005 Paris, France*

**Corresponding authors. E-mails: mezailles@chimie.ups-tlse.fr, sophie.carenco@sorbonne-universite.fr*

ABSTRACT: Bimetallic phosphide nanoparticles are drawing a great interest as a family of nanomaterials. Controlling their fine features such as surface composition, core crystal structure and overall composition is a key to further application. Copper and nickel are particularly interesting first-raw metals for their abundance and relevance in several branches of catalysis. In order to synthesize crystalline bimetallic phosphide Ni-Cu-P nanoparticles, core-shell copper-nickel nanoparticles were reacted with white phosphorus (P_4). Surprisingly, hollow monocrystalline $(Ni,Cu)_2P$ nanoparticles were formed alongside Cu nanoparticles and crystallized in a phase isostructural to Ni_2P. Using a combination of local and ensemble analytic techniques, we showed that this unique structure is the result of several competing processes: phosphorus migration, interaction of stabilizing ligands with copper as well as metal phosphide phase crystallization. This study provides important mechanistic insights to rationalize bimetallic phosphide nanoparticles syntheses. Beyond metal phosphides, this well-characterized case study about competing diffusion and crystallization processes is of major relevance for the advancement of materials sciences at the nanoscale.

1. Introduction

Metal phosphides (M_xP_y) have a large variety of compositions and a wide range of applications in catalysis,[1–3] magnetism,[4–6] lithium-ion batteries,[7–9] as semi-conductors[10–12] and for superconductivity.[13] At the nanoscale, they have also attracted great interest due to their promising performances especially in electrocatalysis[3,14] and photoluminescence[10,12,15] among other applications. While chemists have been initially working on synthesis of monometallic phosphide nanoparticles[15–17], recent efforts have

focused on the controlled synthesis of bimetallic phosphide nanoparticles, which show enhanced properties.[18–21] Most reported studies relied on the non-quantitative decomposition of tri-*n*-octylphosphine (TOP), triphenylphosphine (PPh_3) or triphenylphosphite (TPP) in the presence of metal complexes or salts, thus forming metal phosphide nanoparticles in one step or two steps.[22] To synthesize monometallic phosphides, insertion of phosphorus into preformed nanoparticles was also investigated. This approach allows an excellent control over size, shape and crystalline phase because it preserves the morphology and size-distribution of the starting metal nanoparticles.[23] Nevertheless, this insertion route was rarely used on bimetallic nanoparticles[24] despite the large number of candidates available.[25] Indeed, synthesis of bimetallic nanoparticles, such as Au-Cu, Pt-Pd, Pt-Ni and Cu-Ni[26–29], with tunable composition and precise atomic order control is a mature field.

Copper phosphide and nickel phosphide nanoparticles show good performance in (electro)catalytic processes.[14,30,31] While bulk mixed phosphides of copper and nickel $(Ni,Cu)_3P$ and $(Ni,Cu)_2P$ have been prepared by Nowotny et al. and Adlwarth et al.,[32,33] nanoscaled Cu-Ni-P have been synthesized by solution-based route[34] or by electrical wire explosion.[35] In these last two examples, the nanoparticles crystallized in cubic phases, isostructural to metallic Cu and Ni, and the latter showed low phosphorus content ($\leq$ 8.3 at.%) as well as inhomogeneous composition of individual particles. There is no report so far on Ni-Cu-P nanoscaled phosphides presenting a crystal structure indexed as a metal phosphide. Hence, a strategy that involves insertion of phosphorus into pre-formed Ni-Cu nanoparticles does seem particularly appealing to target Ni-Cu-P nanoparticles by colloidal synthesis.

For this purpose, white phosphorus (P_4) shows several interesting features as a phosphorus donor. It acts as a stoichiometric P-donor for both nickel and copper, forming crystalline Ni_2P and Cu_3P nanoparticles.[17,36] No by-product is produced during the reaction and phosphorus insertion started at temperature as low as 100 °C. Furthermore, it was shown to be a stoichiometric donor in other cases such as Pd_5P_2,[37] PdP_2,[37] FeP[17] or InP.[38] Interestingly, the phosphorus insertion occurred through amorphization of the nanoparticles for nickel and palladium, but not for copper.

Herein, we propose a one-step colloidal route for $Cu_{1-x}Ni_x$ nanoparticles. We investigated the reaction of core-shell $Cu_{0.25}Ni_{0.75}$ nanoparticles with white phosphorus, for the production of crystalline Ni-Cu-P nanoparticles. The stoichiometry was selected to target full phosphidation of Ni into Ni_2P. This study provides insights on three mechanistic aspects: (i) preference of phosphorus towards one of the metals, (ii) amorphization and recrystallization during insertion of phosphorus and (iii) outward migration of copper vs. inward migration of phosphorus.

2. Results and discussion

2.1. Synthesis and characterization of bimetallic $Cu_{1-x}Ni_x$ nanoparticles.

In order to prepare bimetallic $Cu_{1-x}Ni_x$ nanoparticles (x = 0.33, 0.50, 0.67, 0.75), we adapted a synthetic protocol designed for pure nickel nanoparticles.[39] $Cu(acac)_2$ and $Ni(acac)_2$ were reduced at 220 °C by oleylamine, in the presence of tri-*n*-octylphosphine (TOP) that served as a stabilizing agent (see experimental section). The reactions were carried out under inert atmosphere to yield colloidal solutions. Black powders of $Cu_{1-x}Ni_x$ nanoparticles were collected by centrifugation and washing in air. Inductively

coupled plasma with atomic emission spectroscopy (ICP-AES) showed that the final compositions are in good accordance with the expected ones (ESI Table S1).

X-ray diffraction (XRD) pattern of $Cu_{0.25}Ni_{0.75}$ nanoparticles is presented in Figure 1. The nanoparticles crystallized in the same fcc phase as metallic copper and nickel. However, their diffraction peaks were shifted to larger angles compared to Cu and smaller angles compared to Ni (Figure 1a and ESI Figure S1). The (111) peaks were fitted by two pseudo-Voigt curves to identify two components at 43.6 ° and 44.4 ° (Figure 1b). The former was attributed to Cu-rich crystalline domains and the latter to Ni-rich ones. The presence of two components indicated that copper and nickel do not form a single-phase solid solution. XRD patterns of $Cu_{1-x}Ni_x$ nanoparticles ($x = 0.25$, 0.50, 0.67) synthesized with other metal ratios show gradual shifts of all three peaks (111), (200) and (220) to larger angles with increasing nickel content (ESI Figure S1). Cu-rich and Ni-rich phases could be distinguished from the (111) peak of all $Cu_{1-x}Ni_x$ samples. The two components were resolved for $x \geq 0.67$. According to the Scherrer equation, the Ni-rich and Cu-rich crystallite domains were respectively 8 nm and 11 nm large, in average.

Bright-field transmission electron microscopy (TEM) images of $Cu_{0.25}Ni_{0.75}$ showed quasi-spherical nanoparticles with average diameter of 40 nm (Figure 1c). This diameter was larger than the average crystallite size, suggesting that the nanoparticles were polycrystalline. Accordingly, high resolution scanning transmission electron microscopy (HR-STEM) revealed several crystalline domains of *ca.* 10 nm within one particle (ESI Figure S2). TEM images of $Cu_{0.75}Ni_{0.25}$, $Cu_{0.50}Ni_{0.50}$ and $Cu_{0.33}Ni_{0.67}$ nanoparticles are shown in ESI Figure S3. The size distribution of the nanoparticles became broader with increasing copper content. This is likely due to the increasing

copper leaching from copper-rich nanoparticles in the presence of TOP,[40] which fastened the defocusing size ripening of the nanoparticles.

Energy dispersive spectroscopy (EDS) in STEM showed a core-shell structure for the $Cu_{0.25}Ni_{0.75}$ nanoparticles (Figure 1). This partial segregation is compatible with the XRD pattern which indicated two types of crystallites. The core was rich in Cu while the shell was rich in Ni. Based on EDS maps performed on the TEM, apparent ratios could be estimated, although the measurement in the center of the nanoparticle also took into account the shell that is crossed twice by the electron beam. Uncertainty of all the values discussed below is in the order of 10 %. The apparent composition was $Cu_{0.07}Ni_{0.93}$ in the shell and $Cu_{0.46}Ni_{0.54}$ in the core. STEM-EDS maps of $Cu_{1-x}Ni_x$ nanoparticles with others metal ratios showed core-shell morphology as well (ESI Figure S4). In particular, $Cu_{0.33}Ni_{0.67}$ nanoparticles with similar size to $Cu_{0.25}Ni_{0.75}$, showed an apparent composition of $Cu_{0.09}Ni_{0.91}$ in the shell and $Cu_{0.57}Ni_{0.43}$ in the core. As expected, the shell was thinner than that of $Cu_{0.25}Ni_{0.75}$ nanoparticles i.e. 7 nm compared to 10 nm.

The core-shell structure was favored over an alloy or Janus structure, in agreement with the syntheses previously developed in the literature for other copper-nickel nanoparticles.[26,27,28] However, our results differ from the work of Liu et al. who obtained alloys using a similar approach but at a lower temperature i.e. 180 °C and with longer reaction time of 4 h.[41] In our reaction, the solution readily turned dark at *ca.* 180 °C. We know from our previous work that the reduction of $Ni(acac)_2$ starts at 213 °C.[39,42] Hence, we propose that Cu nuclei form at 180 °C and that reduction of nickel at a higher temperature is responsible for the partially segregated morphology.

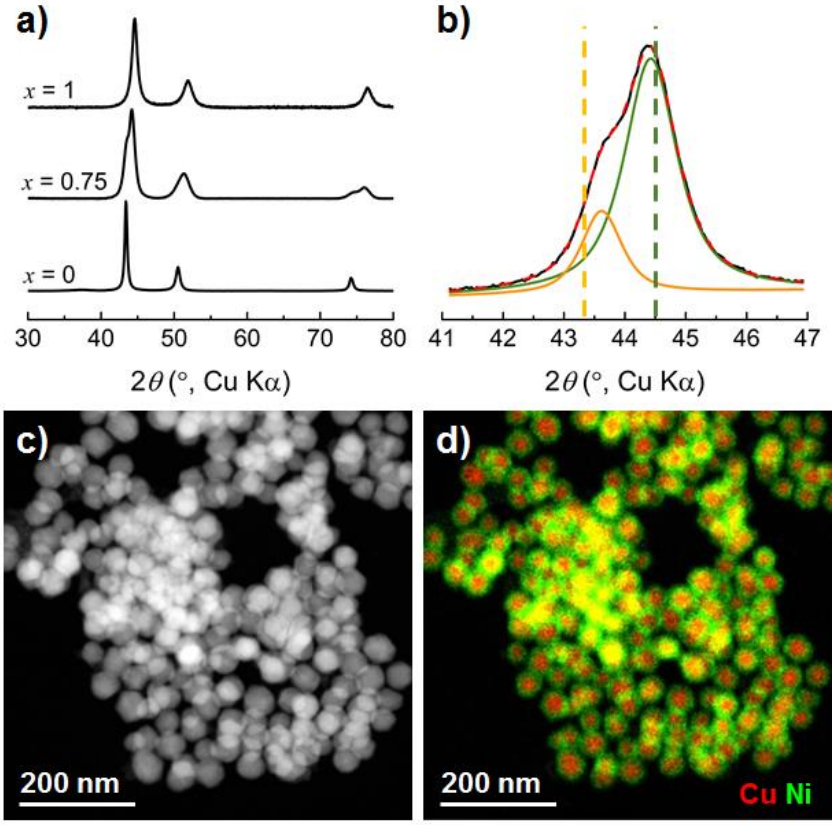

Figure 1: a) XRD patterns of Cu, $Cu_{0.25}Ni_{0.75}$ and Ni nanoparticles. b) Deconvolution of the (111) peak of $Cu_{0.25}Ni_{0.75}$ nanoparticles with its copper-rich component at 43.6° (orange, corresponding to the stoichiometry $Cu_{0.7}Ni_{0.3}$ based on Vegard's law) and nickel-rich component at 44.4° (green, corresponding to the stoichiometry $Cu_{0.1}Ni_{0.9}$ based on Vegard's law). The dotted lines are a guide to the eye for pure copper (orange) and nickel (green). c) STEM-HAADF images of $Cu_{0.25}Ni_{0.75}$ nanoparticles and d) their EDS map.

On the powder of nanoparticles isolated in air, X-ray photoelectron spectroscopy (XPS) of the P 2p region showed the presence of phosphorus species on the surface of the nanoparticles. Each component was represented by $2p_{3/2}$ and $2p_{1/2}$ doublet peaks with a spin-orbit splitting of 0.84 eV. In the following, we will only indicate the binding energy (BE) of the $2p_{3/2}$ component. Three components were identified at 129.4, 132.6 and 133.0 eV (ESI Figure S5b). The component at 129.4 eV, representing 13% of the

total phosphorus content detected at the surface, was attributed to nickel phosphide.[43] This phosphide came from a partial decomposition of TOP and contaminates the surface, in agreement with previous reports.[44,45,46] The component at 132.6 eV was attributed to phosphine oxide,[47,48] originating from oxidation of TOP into tri-*n*-octylphosphine oxide (TOPO) during the post-reaction treatment. Lastly, the component at 133.0 eV was attributed to phosphates, from partial phosphide oxidation.[49] On the metals side, Ni 2p and Cu 2p were measured (ESI Figure S5c and d). Partially oxidized nickel was detected on the surface while no signal of oxidized Cu was detected in the Cu 2p region, in agreement with the proposed structure of a nickel thick shell.

2.2. Phosphorus insertion into core-shell $Cu_{0.25}Ni_{0.75}$ nanoparticles.

Stoichiometric reaction of white phosphorus on copper and nickel nanoparticles was previously reported.[17,36] Using stoichiometric amounts of P_4, crystalline Cu_3P was formed at 100 °C, while Ni_2P only partially crystallized at 150 °C and fully crystallized at 220 °C. Using sub-stoichiometric amounts of P_4, Ni_3P did not crystallize. Rather, nanoparticles with Ni_2P core and metallic Ni shell were obtained. In the case of copper, faster crystallization of the phosphide phase led to nanoparticles with the opposite structure: metallic Cu core and Cu_3P shell.

In this work, core-shell $Cu_{0.25}Ni_{0.75}$ nanoparticles were reacted with P_4 in sub-stoichiometric amount compared to the fully phosphidized Cu_3P-Ni_2P. The chosen stoichiometry of the final product was $Cu_{0.25}Ni_{0.75}P_{0.375}$, corresponding to hypothetical "Cu-Ni_2P". Two borderline scenarios were envisioned (Figure 2): either a diffusion of phosphorus limited to the shell, yielding a metallic core and a phosphide shell, or a diffusion of phosphorus to the core, yielding a bimetallic phosphide alloy. The outcome

would depend on the relative kinetics of crystallization of both phosphide phases and the preference of phosphorus towards one of the metals.

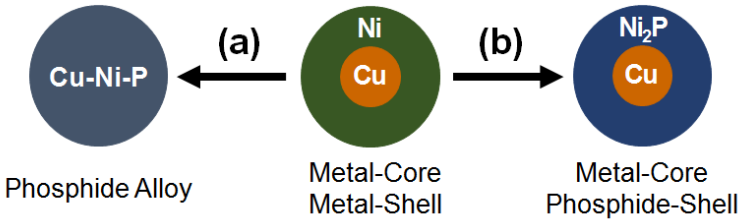

Figure 2: Two borderline scenarios of phosphorus insertion into core-shell Cu-Ni nanoparticle.

(i) Preference of phosphorus towards one of the metals

To obtain a fully crystallized product, as-synthesized $Cu_{0.25}Ni_{0.75}$ nanoparticles were reacted directly after synthesis (no further purification) with a solution of P_4 in toluene at 250 °C for 2 h. Toluene was evaporated *in vacuo* before heating to avoid reflux at the reaction temperature. ^{31}P NMR spectrum of the supernatant after centrifugation shows that P_4 was completely consumed (ESI Figure S7b). TOP remained from the first step of the synthesis and gave a signal at -31.9 ppm (see inset). Two phosphorus species at oxidation degree +V were detected at 43.2 and 43.1 ppm, one of them likely corresponding to TOPO and the other unidentified. Chemical composition of the powder was evaluated by EDS. The measured composition $Cu_{0.22}Ni_{0.78}P_{0.34}$ was comparable to the expected one, indicating a quantitative reaction between the copper-nickel nanoparticles and P_4.

XRD patterns of the resulting nanoparticles showed a phase isostructural to hexagonal Ni_2P as well as fcc metallic Cu (Figure 3). Diffraction peaks of the phosphide phase were shifted from those of the reported Ni_2P (JCPDS 74-1385). Peaks of (hkl) ($l \neq 0$) planes were shifted towards wider angles while those of (hkl) ($l = 0$) planes were shifted towards smaller angles, suggesting a distortion of the unit cell. We therefore propose the

formation of a mixed phosphide $(Ni,Cu)_2P$ phase, with a partial substitution of copper to nickel in the unit cell resulting in the structural distortion.

To further substantiate this proposal, we went back to the few articles discussing these structural parameters. Distortion of the unit cell is often discussed using the ratio *c*/*a* of lattice parameters.[50] Nowotny et al. reported that macroscopic $(Ni,Cu)_2P$ phase can form for Cu:Ni ratios up to *ca*. 25%.[32] Measurement uncertainty of our XRD data is around 0.001 nm for distances (this value depends on the angle, see Supporting Information page S15). At 25% Cu, lattice constants showed slightly deviated values of $a = 0.584$ nm and $c = 0.340$ nm from those of pure Ni_2P phase ($a = 0.586$ nm and $c = 0.338$ nm). The resulting *c*/*a* ratio was 0.582 *vs.* 0.577 for pure Ni_2P. In our case, profile matching of the XRD pattern showed lattice constants of $a = 0.591$ nm and $c = 0.333$ nm, giving a *c*/*a* ratio of 0.563. This indicated a more significant distortion at the nanoscale. Interestingly, as the *c*/*a* ratio decreased from that of pure bulk Ni_2P phase, the distortion was also not of the same direction as in the bulk mixed phase (where the *c*/*a* ratio increases). We calculated the *c*/*a* ratio in nanoscale $(Ni,Fe)_2P$ or $(Ni,Co)_2P$ reported by another group, and it showed increasing values when compared to the pure hexagonal Ni_2P phase (ESI Table S3).[20,21] To the best of our knowledge, the $(Ni,Cu)_2P$ distortion reported in this article is the first example of decreasing *c*/*a* ratio for mixed phosphide phase.

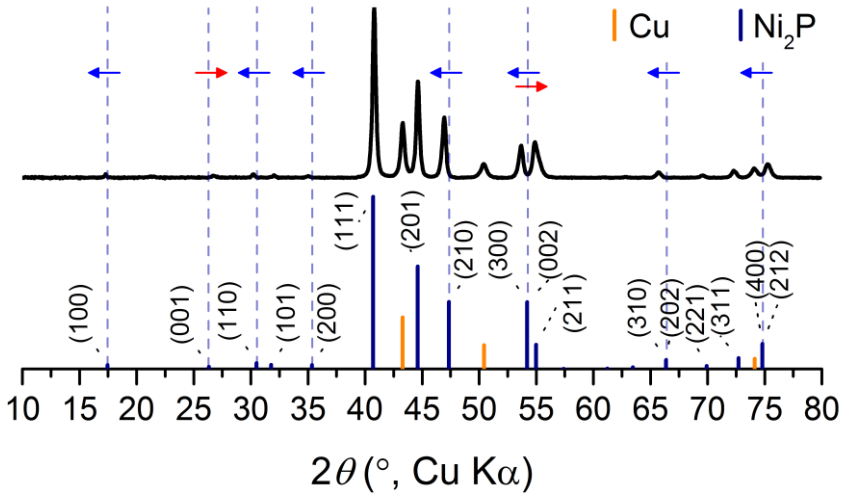

Figure 3: XRD patterns of $Cu_{0.25}Ni_{0.75}$ nanoparticles after reaction with P_4 at 250 °C. Reference patterns of Ni_2P (JCPDS 74-1385) and Cu (JCPDS 04-0836) are in blue and orange. The blue and red arrows are a guide to the eye for visually remarkable shifts of diffraction peaks towards smaller and wider angles respectively. *NB:* The same figure with a logarithmic scale, more appropriate to visualize the smaller diffraction peaks, is available in Figure S13.

At this point, detection of metallic copper and of a bimetallic phosphide phase suggested a reaction closer to scenario (b) (Figure 2). This reasoning was shattered by TEM images that show a majority of hollow nanoparticles (Figure 4a). These hollow nanoparticles were monocrystalline (ESI Figure S8) whereas the starting nanoparticles were polycrystalline. This indicated that the nanoparticles were amorphized at an intermediate step, which will be studied in the next section. Lattice fringes with spacing of 0.51 nm were observed, corresponding to (100) crystal planes of the hexagonal Ni_2P phase (Figure 4b). STEM-EDS showed that the hollow phosphide nanoparticles contained both Cu, Ni and phosphorus, in agreement with the proposed mixed phosphide $(Ni,Cu)_2P$ phase (Figure 4e-h). This was also confirmed by elemental profiles of a delineated zone across a hollow nanoparticle (ESI Figure S6). Alongside the hollow

phosphide nanoparticles, higher contrast zones were also observed, either inside the shells or on top of them (Figure 4a,c,d). EDS elemental maps indicate that they did not contain phosphorus (Figure 4g), but only Cu. They were therefore the metallic copper crystallites determined in the XRD pattern.

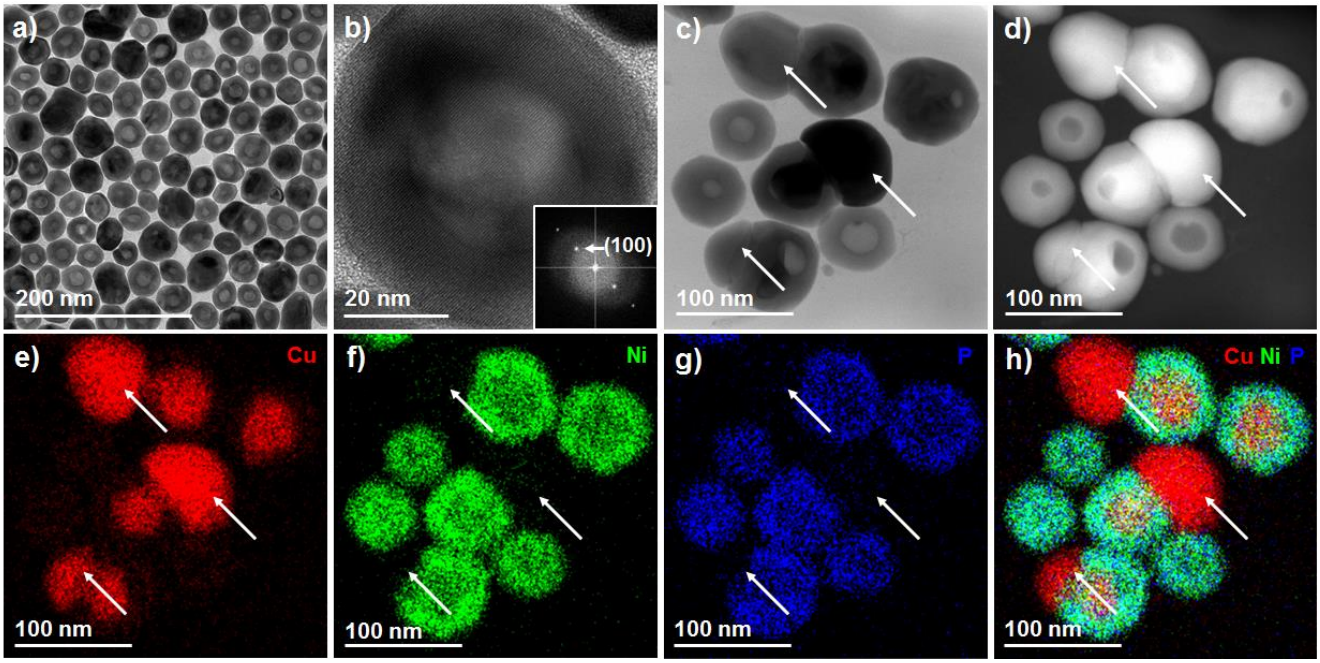

Figure 4: a) TEM image of $Cu_{0.25}Ni_{0.75}$ nanoparticles after reaction with P_4 at 250 °C. b) TEM image of a hollow nanoparticle. Inset: FFT of the image. c) STEM bright-field and d) STEM-HAADF images of a selected zone at higher magnification. e-g) Single-element STEM-EDS maps describing the distribution of Cu, Ni and P, respectively. f) Merged STEM-EDS elemental map. The arrows indicate copper nanoparticles deposited outside the phosphide nanoparticles.

XPS of the nanoparticles powder in the Cu 2p region (ESI Figure S5d) showed the presence of metallic and oxidized Cu, confirming EDS observations. The lower B.E. of the Cu 2p peak could also partially arise from the copper phosphide, as the reported compound show similar binding energies for $Cu^{(0)}$ (932.7 eV), Cu_3P (932.8 eV)[51] and CuP_2 (between 932.2 and 932.4 eV).[52]

In the Ni $2p_{3/2}$ region, peaks of oxidized nickel were present at 855.2 and 855.9 eV.[53] Reduced nickel was also detected at 852.9 eV (ESI Figure S5c). It was slightly shifted to higher binding energy (B.E.) than bimetallic copper-nickel nanoparticles whose main peak was at 852.3 eV. Unfortunately, $Ni^{(0)}$ and Ni_2P are hardly distinguished by XPS. Previous study by Li et al. attributed them the same B.E. of 853.1 eV,[54] while others tabulate $Ni^{(0)}$ at 852.7 eV and Ni_2P at 852.9 eV, only 0.2 eV apart.[55]

XPS relative peak area indicated an apparent surface coverage of copper *vs.* nickel of one third of copper for two third of nickel, much richer in copper than what was found on the nanoparticles prior to phosphidation. This indicated that most of the copper migrated to the surface or to the outside of the nanoparticles, forming aggregates on their own, in agreement with STEM-EDS analysis. Besides, the apparent ratio of surface phosphorus *vs.* the sum of the metals was ca 60%, while it was only 30% prior to the reaction with white phosphorus. Oxidized phosphorus species, similar to these of the starting nanoparticles, were still detected in the form of TOPO and phosphates at 132.8 and 133.2 eV respectively. P 2p indicated the presence of metal phosphide at 129.5 eV,[43] representing 33% of the surface phosphorus (ESI Figure S5b). A minor component was also detected at 130.2 eV, representing 14%. This was assigned to a different reduced phosphorus species as the B.E. value is close to that of metal phosphide. Altogether, XPS confirmed the formation of surface metal phosphide on the nanoparticles and the presence of metallic copper on the surface of the nanoparticles and/or as separate nanoparticles.

The formation of hollow $(Ni,Cu)_2P$ nanoparticles and metallic Cu nanoparticles suggested an outward migration of copper from the core to the shell and even outside of the starting nanoparticles during the reaction with P_4, a scenario that was not initially

envisioned. Moreover, phosphorus showed a preference towards nickel as shown by STEM-EDS and XRD, possibly due to the initial core-shell morphology where nickel was in contact with the reaction medium.

(ii) Amorphization and recrystallization during insertion of phosphorus

As mentioned above, bimetallic copper-nickel nanoparticles likely underwent amorphization during phosphorus insertion. This hypothesis is made based on previous observations on the phosphidation of crystalline nickel nanoparticles by white phosphorus, for which we demonstrated the formation of an amorphous intermediate even when a low stoichiometry of phosphorus was reacted (down to 0.25 P equiv. *vs.* Ni).[36] This was expected because there is no topotactic transformation possible from Ni fcc to hexagonal Ni_2P.[56] A fully amorphous nickel phosphide compound, showing a broad peak from 40 to 50 ° in XRD, was isolated at low temperature (90 °C).[17] In the present case, nickel is exposed at the surface of the nanoparticles and has to react first with P_4.It would thus make sense that the first step of the reaction was the formation of a nickel phosphide amorphous shell.

In order to investigate the reaction mechanism, including the surprising and unprecedented outward diffusion of copper, a second reaction was performed on the $Cu_{0.25}Ni_{0.75}$ nanoparticles, with the same stoichiometry of P_4, but at a lower temperature of 150 °C. ^{31}P NMR spectrum of the supernatant after centrifugation showed again that P_4 was entirely consumed, suggesting a complete conversion (ESI Figure S7c). Indeed, only TOP and TOPO were detected at -31.2 and 44.2 ppm. EDS indicates a chemical composition of $Cu_{0.23}Ni_{0.77}P_{0.43}$, comparable to these of the product formed at 250 °C if one takes into account the experimental error of EDS (*ca.* 5%) and the fact that the

phosphorus-containing ligands (of variable amount from sample to sample) contribute to the overall phosphorus amount.

The isolated powder was partially amorphous as shown by XRD (Figure 5a) through a broad feature from 40 to 50 °. This feature may correspond to amorphous nickel phosphide[17,36] but also to amorphous copper phosphide or copper-nickel phosphide. The diffractogram also presented diffraction peaks of hexagonal Ni_2P and fcc metallic Cu. This confirmed a two-step process with first, an amorphization driven by phosphorus insertion and/or copper migration, and second, a recrystallization. Interestingly, no shift was observed for the diffraction peaks of the Ni_2P phase: pure Ni_2P phase seems to crystallize first, before evolving towards mixed $(Ni,Cu)_2P$ phase as a consequence of copper outward migration.

In order to confirm this, the obtained partially amorphous nanoparticles were re-dispersed in oleylamine and annealed at 250 °C for 2 h. As expected, XRD pattern of the annealed product showed crystalline $(Ni,Cu)_2P$ alongside fcc metallic copper, but no broad signal resulting from an amorphous phase. However, diffraction peaks of the mixed phosphide phase were more shifted compared with these of Ni_2P, than in those of the nanoparticles formed at 250 °C. In fact, the *c*/*a* ratio decreases to 0.559.

TEM of the sample synthesized at 150 °C showed full and partially hollow nanoparticles, alongside hollow nanoparticles (Figure 5b). This suggested that outward migration of copper already started and was still undergoing at this temperature. Surprisingly, no significant morphology change was observed in the annealed sample (Figure 5c): copper crystallites were not observed outside the nanoparticles. Isolating the nanoparticles after the first reaction step at 150 °C seems to deactivate the outward migration of copper. This isolation step removed most of the TOP from the reaction

medium: initially 0.8 equiv. *vs.* the metals, which represents a large excess *vs.* the surface metal atoms. We recently showed that alkylphosphines are responsible for strong leaching of copper nanoparticles to solution.[40] Hence, we propose that, for the one-step reaction described in the previous section, the presence of TOP in the reaction medium was a significant driving force for the outward migration of copper by displacing the equilibrium in the favor of soluble copper species. These species were then able to redeposit on the metal phosphide nanoparticles, as will be discussed in detail in the last section of the article.

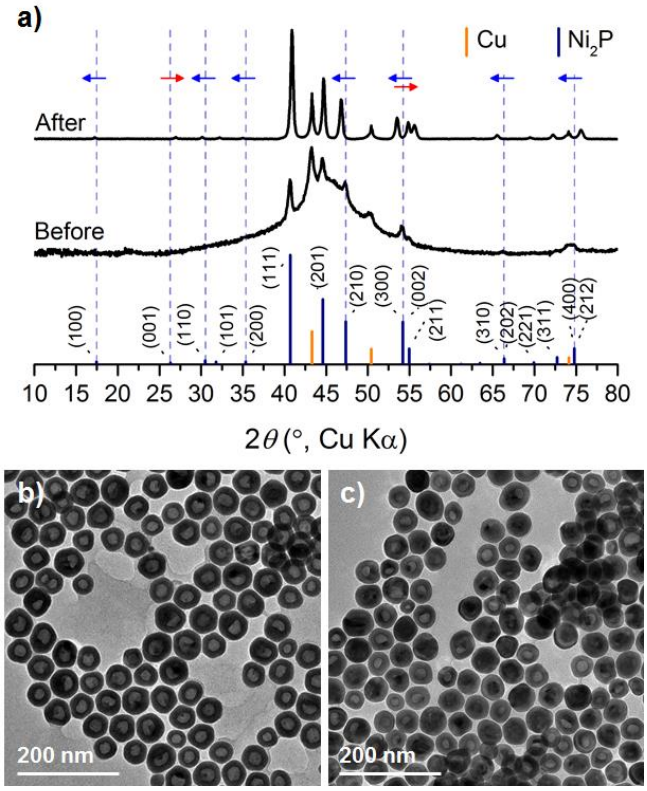

Figure 5: a) XRD patterns of the nanoparticles formed after reaction with P_4 at 150 °C before and after annealing in oleylamine at 250 °C for 2 h. Reference patterns of Ni_2P (JCPDS 74-1385) and Cu (JCPDS 04-0836) are in blue and orange. The blue and red arrows are a guide to the eye for significant shifts of diffraction peaks towards smaller and wider angles, respectively. *NB:* The same figure with a logarithmic scale, more appropriate to visualize the

smaller diffraction peaks, is available in Figure S14. b) and c) TEM images of the nanoparticles before and after annealing, respectively.

STEM-EDS elemental maps of the 150 °C sample showed that the nanoparticles react inhomogeneously with P_4 (Figure 6), providing an unexpected opportunity to catch snapshots of the reaction steps on the same TEM grid. Four different stages of phosphorus insertion could be distinguished, numbered intermediates (1) to (4) (Figure 6f-g). As shown in phosphorus STEM-EDS map (Figure 6e), for intermediate (1), phosphorus insertion was incomplete and stopped at the surface of the nanoparticle, whereas, for intermediates (2) to (4), phosphorus completely occupied the shell of the nanoparticles. Phosphorus diffusion always stopped at the shell and never continued into the core. This confirmed our previous conclusion on the preference of phosphorus towards nickel rather than copper in this system.

The copper map (Figure 6c) showed that the core of intermediates (1) and (2) were still intact while intermediates (3) and (4) were partly and fully hollow, respectively. Interestingly, the shell of intermediates (2) to (4) always contained the three elements, suggesting the presence of amorphous bimetallic phosphide, detected as a broad amorphous species by XRD below the crystalline Ni_2P (Figure 5a). The amorphous nature of these intermediates was confirmed by Selected Area Electronic Diffraction (SAED) (ESI Figure S9). This indicated that there are two competing reaction pathways: a first where crystalline Ni_2P formed first then evolved towards mixed $(Ni,Cu)_2P$ through copper migration and a second where copper migration occurred first to form amorphous mixed phosphide that crystallized afterward, at 250 °C.

XPS of the non-annealed sample in the Cu 2p and Ni 2p regions showed again the presence of both reduced and oxidized species (ESI Figure S5). While comparing with

the sample formed at 250 °C, the apparent copper content measured at the surface increased from 14% to 25% and the nickel content decreases from 27% to 14%. This is likely due to the fact that outward migration of copper was still undergoing. We detected both remaining copper inside the shell or small copper species outside. P 2p region of the non-annealed was also similar to that of the sample formed at 250 °C (ESI Figure S5).

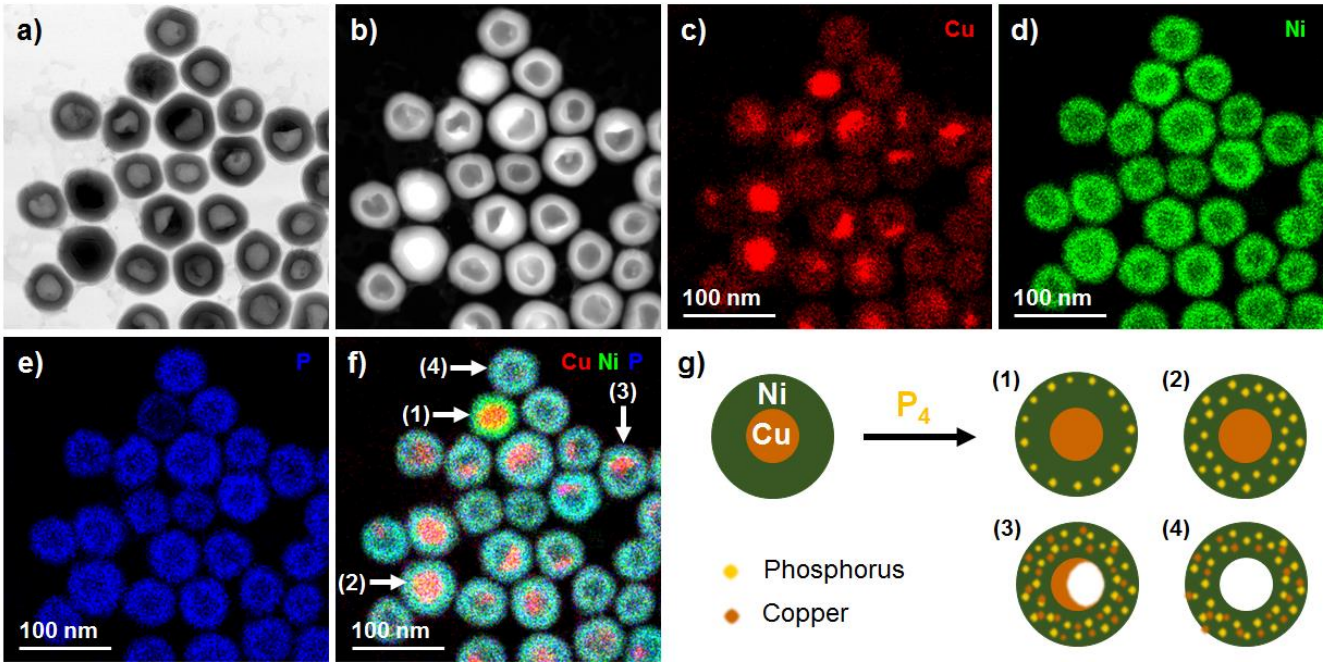

Figure 6: a) STEM bright-field and b) STEM-HAADF images of the nanoparticles after reaction with P_4 at 150 °C. c-e) Single-element STEM-EDS maps describing the distribution of Cu, Ni and P, respectively. f) Merged STEM-EDS elemental map. g) Schematic illustrations of different stages of phosphorus insertion.

(iii) Outward migration of copper vs. inward migration of phosphorus

In order to determine the fate of copper that migrated outward the nanoparticles, and potentially/partially outside, during the reaction with white phosphorus at 250 °C, TEM images of aliquots from the reaction mixture were taken at different reaction times

(Figure 7). As expected, the nanoparticles were still not hollow at room temperature (Figure 7a). The majority of the nanoparticles was already hollow at 180 °C (Figure 7b), consistently with the TEM of nanoparticles prepared at 150 °C shown in the previous section. When the temperature reached 250 °C, small nanoparticles of diameter of around 4 nm were detected outside of the hollow nanoparticles (Figure 7c). After 30 min at this temperature, larger particles were found (Figure 7d), consistent with our observation of copper nanoparticles by STEM-EDS in the final product (Figure 4). Outward migration of copper eventually resulted in nucleation and growth of copper nanoparticles outside of hollow phosphide nanoparticles.

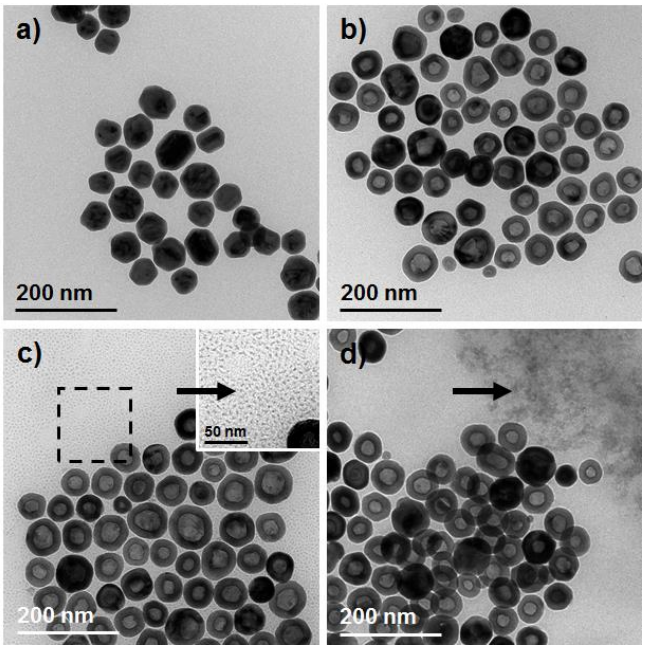

Figure 7: TEM images of the nanoparticles during the reaction with P_4 at 250 °C. The sample was taken at a) room temperature, b) 180 °C during the heating ramp, c) when the temperature reached 250 °C (inset is an image at higher magnification of the squared region), d) after 30 min at 250 °C. The arrows indicate smaller nanoparticles outside the larger ones.

The migration of copper outside the nanoparticles was further confirmed using *in situ* STEM-EDS mapping (Figure 8). As discussed above, the sample formed after reaction

with white phosphorus at 150 °C presented several intermediates of phosphorus insertion (Figure 6). Thus, we heated this sample under argon (1 bar) from room temperature up to 250 °C in a TEM gas cell. This experiment was slightly different than heating in solution, but since copper easily migrates on the silicon nitride membrane upon heating, we considered it a worthwhile comparison experiment. As expected, STEM images showed that the thickness of the core decreases from 18 nm to 6 nm between 100 °C (Figure 8a,c) and 250 °C (Figure 8b,d). Moreover, STEM-EDS elemental maps showed the copper migrating to the outside of the nanoparticles and redepositing nearby, from Figure 8e to Figure 8f.

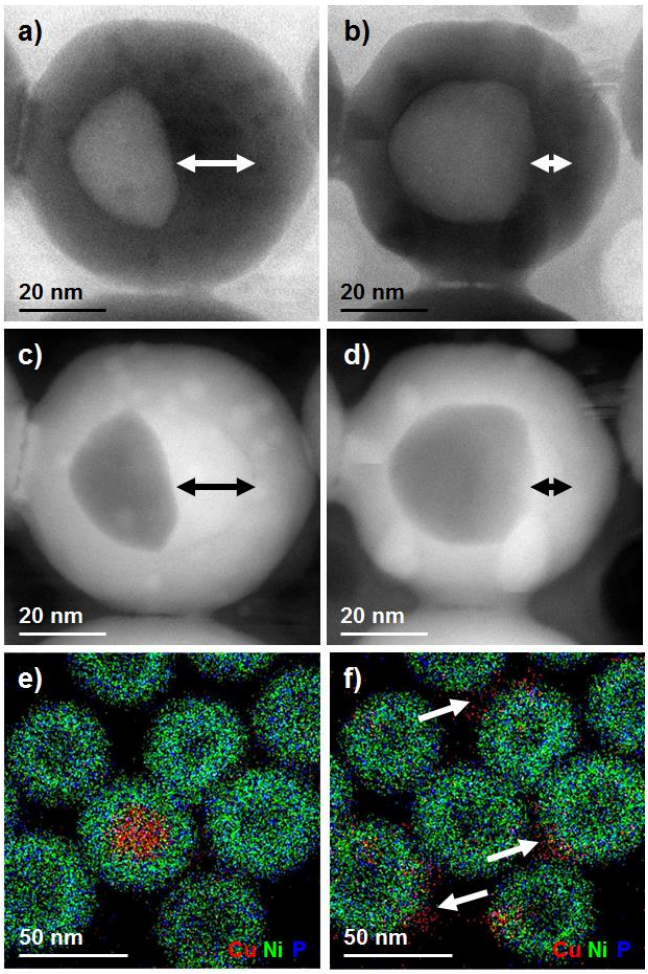

Figure 8: *In situ* annealing of the nanoparticles formed after reaction with P_4 at 150 °C. STEM bright-field images of the nanoparticles heated *in situ* under argon at a) 100 °C and b) 250 °C. c) and d) their respective STEM-HAADF. The arrows indicate the core thickness. Merged STEM-EDS elemental maps of the nanoparticles heated *in situ* under argon at e) 100 °C and f) 250 °C. The arrows indicate deposited copper outside the hollow nanoparticles.

We showed that the inward migration of phosphorus and outward migration of copper already started at 150 °C when the core-shell copper-nickel nanoparticles were reacted with white phosphorus. However, between 150 and 250 °C, it was shown that TOP could also act as a phosphorus source for insertion into metal.[44–46] A control reaction was thus carried out at 180 °C in the same fashion without adding white phosphorus. The only phosphorus source for insertion in this case was the TOP remaining from the

first step of the bimetallic nanoparticle synthesis. No change in size, shape, crystal structure, chemical composition as well as apparent copper content measured on the surface of the nanoparticles was observed after the heating (ESI Figure S10), confirming that P_4, as a more reactive P-donor, is required to activate outward migration of copper at 180 °C.

We then carried out a second control reaction at 250 °C. This time, XRD pattern of the sample showed pure orthorhombic phosphide $Ni_{12}P_5$ and fcc metallic copper phases (ESI Figure S11), indicating phosphorus insertion. Chemical composition measured by EDS confirmed enrichment in phosphorus (ESI Figure S11). Interestingly, TEM images and STEM-EDS mapping showed full and faceted nanoparticles alongside only a few hollow nanoparticles (ESI Figure S11 and Figure S12). No copper was detected outside of the nanoparticles. XPS only showed very small apparent Cu-content (3 at.% of total Cu, Ni and P) on the surface (ESI Figure S11). The high-temperature degradation of TOP seems to inhibit copper migration, directly resulting in a crystalline phosphide shell.

2.3. Discussion

(i) Regarding the preferred formation of nickel-rich phosphide over copper-rich phosphide.

Overall, the above paragraphs describe the formation of a nickel-rich NiCuP alloy. While some of the copper domains are not phosphidized, there is no remaining nickel domain at the end of the reaction. This suggests a preference of phosphorus for the nickel rather than for the copper.

Two aspects can be considered:

(1) The reaction path. Due to the core-shell morphology of the starting nanoparticles, phosphorus reacts first with nickel. The nickel phosphide, once formed, traps a significant amount of the available phosphorus species. This should however be reconciled with the fact that copper is able to diffuse through the nickel-rich phosphide shell. Kinetic control cannot be solely responsible for the observed result.

(2) The stability of the final phases. Data are not available on the ternary alloys but they are for the binary ones: the enthalpy of formation of Ni_2P at 298 K (from -190 to -136 kJ/mol depending on the studies) is more negative than these of Cu_3P (from -52 to -135 kJ/mol).[57] At the nanoscale and using the most reactive phosphorus source available (P_4), we can also note that nickel nanoparticles fully convert in Ni_2P nanoparticles at a lower temperature (150 °C) than these required to convert Cu nanoparticles in Cu_3P ones (250 °C or at least above 220 °C).[17] These two arguments suggest a higher stability of nickel-rich phosphide over copper-rich ones.

To further advance this discussion, it would be interesting to perform the reaction of P_4 with a nickel-copper alloy or with an inverted core-shell (nickel inside, copper outside) and to measure the enthalpy of formation of the ternary alloys. Both go beyond the scope of this study. Also, a more systematic phosphidation study (preferably using a stoichiometric P donor) on other bimetallic nanoparticles (eg. NiPd) would be interesting, in order to eventually propose a general rule or law regarding the selectivity of the phosphidation reaction.

(ii) Regarding the formation of hollow nanostructures.

The formation of hollow nanostructures was previously observed for a number of materials, including metal oxides (as a result of oxidation reaction from O_2),[48,58] metal

sulfides (due to sulfidation, eg. from S_8)[59] and phosphides (due to phosphidation, eg. from TOP[23] or from P_4).[17,60] The holes result from the coalescence of vacancies in the center of the nanoparticles. The vacancies are generated as the inner element (typically, the metal) diffuses outward faster than the outer element (typically, sulfur, oxygen, phosphorus) diffuses inward. It is often called "nano-Kirkendall" effect due to the phenomenological similitude with the original Kirkendall effect, which is the appearance of vacancies at the interface of two metals *A* and *B*, as a consequence of unbalanced diffusion coefficients of *A* toward *B* vs. *B* toward *A*.[61]

In the present case, the closest phenomenon related to a Kirkendall effect would have been the formation of vacancies at the copper-nickel interface due to unbalanced nickel and copper diffusion rates. Such phenomenon could be expected at a high enough temperature because the nickel diffuses slower in copper than the copper in the nickel, as well as in copper-nickel alloys.[62] Here, the situation is different: the copper outward diffusion is a consequence of the reaction with an external non-metallic element: phosphorus. For clarity, we will hence avoid the term "nanoscale Kirkendall effect".

Under fairly similar reaction conditions, the phosphidation of single-metal nanoparticles of nickel or copper did not yield hollow nanoparticles in our previous studies.[17] It should be noted that the study on the copper nanoparticles was performed in the absence of phosphine ligands. Based on these observations, we propose that:

(1) Nickel-rich NiCuP alloy allows the diffusion of Cu from the inside to the outside. This is especially well observed *in situ* (Figure 8).

(2) The formation of copper-phosphine species likely acts as a driving force for the copper migrating outside of the nanoparticles, as was also observed by Robinson and

coworkers on copper sulfide nanoparticles.[63] Such copper-phosphine species were partly described in a previous work as complexes such as $Cu(PR_3)_2$ and clusters.[40]

3. Conclusions

In this work, we studied the reaction between core-shell copper-nickel nanoparticles (Cu:Ni in 1:3 ratio) and white phosphorus. Surprisingly, we obtained hollow Ni-rich phosphide nanoparticles and Cu nanoparticles, suggesting a preference of phosphorus towards nickel rather than copper in this particular case. The phosphide nanoparticles were shown to crystallize in a mixed $(Ni,Cu)_2P$ phase isostructural to Ni_2P for the first time. Partial substitution of Ni atoms by Cu atoms in the structure leads to a distortion of the unit cell. The lattice constant ratio *c*/*a* decreases from 0.577 (pure Ni_2P) to 0.563, in contrast with other reported Ni-containing bimetallic phosphide nanoparticles.[20,21]

From a mechanistic point of view, we showed that phosphorus insertion into the bimetallic nanoparticles triggers amorphization of the latter as well as outward migration of copper to leave a void in the core (Figure 9). During the outward migration of copper, two competing reaction pathways can occur. Either an amorphous intermediate of $(Ni,Cu)_2P$ forms first and crystallizes into mixed phosphide and/or pure Ni_2P forms first and evolves towards $(Ni,Cu)_2P$. Lastly, the copper that migrates outside the nanoparticles crystallizes into metallic fcc Cu nanoparticles.

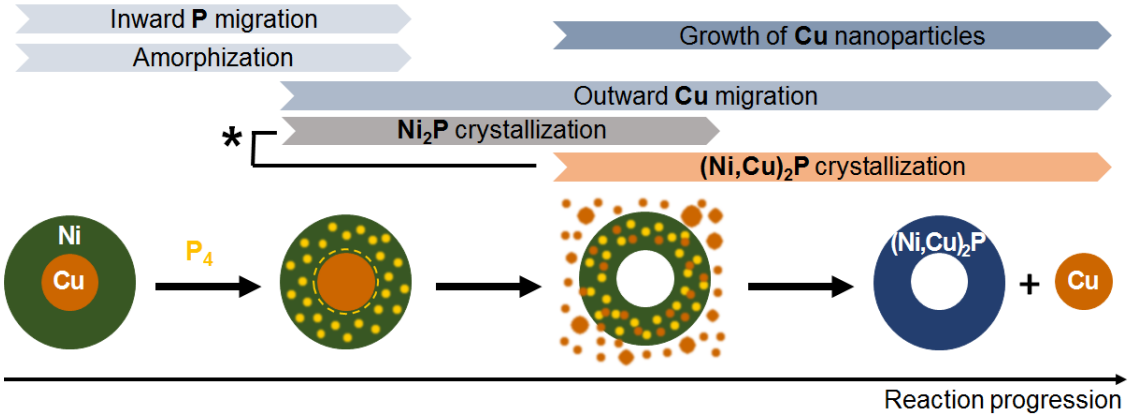

Figure 9: Formation mechanism of hollow mixed phosphide $(Ni,Cu)_2P$ nanoparticles. The asterisk indicates two possible and competing pathways.

The low-temperature reactivity of white phosphorus promotes outward migration of copper while in the case of high-temperature degradation of TOP, the core-shell nanostructure of the starting bimetallic nanoparticles is mostly preserved. The resulting relative kinetics between copper migration and crystallization of the phosphide allows formation of a mixed phosphide $(Ni,Cu)_2P$ phase which is not observed when TOP is used as a sole source of P. The mixed phosphide nanoparticles were monocrystalline and faceted to expose the (001) surface, which is known to be active in HER,[14] opening an avenue for further use of these unique structures as electrocatalysts.

This study of the phosphorus insertion into bimetallic nanoparticles using white phosphorus underlines the competing processes occurring during the reaction. These results from the interaction of stabilizing ligands with copper, as well as phosphorus migration and phosphide phase crystallization. Using a combination of local and ensemble analytic techniques, a complete rationalization of these processes is presented for the first time, in the case of bimetallic copper-nickel nanoparticles. This study paves the way for mechanistic studies of other bimetallic phosphide nanoparticles syntheses.

Electrocatalytic activity of this new type of bimetallic metal phosphide is currently being assessed in our laboratories.

Experimental section

Chemicals. Oleylamine (OAm; technical grade, 70%) was purchased from Sigma-Aldrich. Tri-*n*-octylphosphine (TOP; 97%), copper (II) acetylacetonate ($Cu(acac)_2$; 98+%) and nickel (II) acetylacetonate ($Ni(acac)_2$; anhydrous, min. 95%) were purchased from Strem Chemicals and stored in the glovebox. All chemicals described above were used without further purification. White phosphorus (P_4) was taken from the laboratory's own chemical stockroom and was dissolved in toluene. A typical P_4 solution has a concentration around 0.4 mol/L in P.

Safety note: White phosphorus is stable in water but highly flammable and toxic if swallowed or inhaled. It is incompatible with oxidizing agents, reducing agents and bases. It is light and heat sensitive and should be handled accordingly.

Synthesis of $Cu_{1-x}Ni_x$ Nanoparticles. Bimetallic copper-nickel nanoparticles were prepared *via* a solvothermal reaction under either purified argon or nitrogen atmosphere using standard air-free techniques with Schlenk line. In a typical synthesis of $Cu_{0.25}Ni_{0.75}$, $Cu(acac)_2$ (0.51 g, 1.95 mmol, 0.25 equiv.), $Ni(acac)_2$ (1.50 g, 5.85 mmol, 0.75 equiv.) and 2.80 mL of TOP (6.24 mmol, 0.8 equiv.) were added to 20.8 g of OAm (78.0 mmol, 10 equiv.) in a 100 mL three-necked flask at room temperature. For nanoparticles with other Cu/Ni ratios, the quantity of each metal precursor was changed in a way that keeps the total amount at 7.80 mmol. The mixture was degassed under vacuum for 5 min then heated to 220 °C, giving quickly a black solution. The solution

was stirred at this temperature for 2 h under inert atmosphere. After heating, it was left to cool to room temperature. The nanoparticles were isolated using acetone and were washed at least three times using a THF/ethanol (1/4) mixture to remove the remaining reagents and organic matter. 465 mg of black powder were obtained, which corresponds to a 100 % yield of $Cu_{0.25}Ni_{0.75}$ (this calculation neglects the weight of organic ligands).

Reaction of $Cu_{0.25}Ni_{0.75}$ Nanoparticles with White Phosphorus. The prepared bimetallic copper-nickel nanoparticles were not isolated before the reaction with white phosphorus. The crude solution from the first step was used as such. For a $Cu_{0.25}Ni_{0.75}P_{0.375}$ stoichiometry, 8.6 mL of a P_4 solution in toluene at 0.34 M in P (2.9 mmol, 0.375 equiv.) were added to the crude reaction mixture of the synthesis of $Cu_{0.25}Ni_{0.75}$. The mixture was degassed under vacuum for 30 min to eliminate the toluene. It was heated to 250 °C for 2 h under inert atmosphere then was left to cool to room temperature. The nanoparticles were isolated using the same method as for bimetallic nanoparticles. Supernatant from the first centrifugation were collected to analyze with ^{31}P NMR. Syntheses with different quantities of P_4 and temperature were carried out in the same fashion.

Control Reaction of $Cu_{0.25}Ni_{0.75}$ Nanoparticles with White Phosphorus. The reaction medium of a typical $Cu_{0.25}Ni_{0.75}$ nanoparticles synthesis was left to cool to room temperature. It was then heated to 250 °C for 2 h under inert atmosphere. The work-up procedure was done in the same fashion as in the actual reactions with white phosphorus.

Annealing of $Cu_{0.25}Ni_{0.75}P_{0.375}$ Nanoparticles. Previously isolated $Cu_{0.25}Ni_{0.75}P_{0.375}$ nanoparticles were re-dispersed in 15 g of OAm. The mixture was degassed under vacuum at 50 °C for 15 min then heated to 250 °C. The black solution was stirred at this

temperature for 2 h under inert atmosphere. The nanoparticles were isolated using the same method as for bimetallic nanoparticles.

X-ray Diffraction. Powder XRD measurements were performed with a Bruker D8 X-ray diffractometer operating in the reflection mode at Cu Kα radiation with 40 kV beam voltage and 40 mA beam current. Typical diffraction patterns were collected with steps of 0.05° and a scanning speed of 2.5-5 s/point. For easier phase identification, the background was subtracted using EVA software. Profile matching of diffraction patterns was carried out using the Thompson-Cox-Hastings pseudo-Voigt function model with Fullprof program.

Conventional Transmission Electron Microscopy. TEM were recorded on a TECHNAI G2 Spirit microscope operating at 120 kV. Samples were prepared by evaporating a drop of *n*-hexane diluted nanoparticles suspension on a carbon-coated copper grid.

Scanning Transmission Electron Microscopy, elemental mapping by Energy Dispersive Spectroscopy and *in situ* experiments. STEM bright-field and HAADF, STEM-EDS and *in situ* observations were performed using a spherical aberration corrected JEOL 2100 F operating at 200 kV. EDS mapping was performed using JEOL Silicon Drift Detector (DrySD60GV: sensor size 60 mm^2) with a solid angle of approximately 0.5 srad. For the acquisition of EDS maps, molybdenum grids were used to prevent the unsuited contribution of the traditional copper TEM grids to the Cu signal originating from the nanoparticles. *In situ* STEM annealing of $Cu_{0.25}Ni_{0.75}P_{0.375}$ nanoparticles was carried out using the Atmosphere device purchased from Protochips Inc. (Raleigh, NC, USA).[64] The sample was placed between two micro-electrical-mechanical systems (MEMS)-based closed cell (SiN windows). The temperature and

the gas flow in the cell were controlled by the heating holder and a gas delivery manifold. The samples were dispersed in *n*-hexane and drop-casted on the SiN membrane. The *in situ* experiments were done at atmospheric pressure under Ar. Four temperatures were chosen for the observations: 100, 150, 200 and 250 °C. At each temperature, the ramp duration was 20 min and the heating rate was 5 °C/min.

Energy Dispersive X-ray Spectroscopy. A small amount of powder was deposited on carbon adhesive tape on a scanning electron microscope sample holder. EDS analyses were performed on a SEM HITACHI S-3400N instrument at 20 kV. Cobalt was used as calibrator and the analyses were performed on at least three different zones on the samples to calculate an average chemical composition.

Nuclear Magnetic Resonance Spectroscopy. ^{31}P liquid NMR spectra were recorded on a Bruker AC-300 SY spectrometer. Chemical shifts are relative to an 85% H_3PO_4 external reference. P_4 was detected as a singlet at -521 ppm.

X-ray Photoelectron Spectroscopy. Spectra were collected on a Omicron Argus X-ray photoelectron spectrometer, using a monochromated Al Kα ($h\upsilon$ = 1486.6 eV) radiation source having a 300 W electron beam power. The samples were analyzed under ultra-high vacuum conditions (10^{-8} Pa). After recording a broad range spectrum (pass energy 100 eV), high resolution spectra were recorded for the C 1s, Cu 2p, Ni 2p, P 2p core XPS levels (pass energy 200 eV). The binding energies were calibrated with respect to the C_{1s} peak at 284.8 eV. Spectrum processing was carried out using the CasaXPS software package.

Conflict of interest

There is no conflict to declare.

Acknowledgements

Sorbonne Université, CNRS, and the Collège de France are acknowledged for financial support. Labex MATISSE is acknowledged for funding the master thesis (ANR-11-IDEX-0004-02). The authors acknowledge financial support from the CNRS-CEA "METSA" French network (FR CNRS 3507) for the TEM experiments. We thank Isabelle Génois and Mohamed Selmane for the help with EDS measurements and profile matching of XRD patterns.

Supporting Information

Supporting information available: complementary data on the nanoparticles before and after reaction (XRD, HR-STEM, STEM-EDS, XPS, ICP-AES, NMR). Figures 3 and 5a redrawn in logarithmic scales. This material is available free of charge via the internet at http://pubs.acs.org.

Table of content entry

Phosphidation of core-shell CuNi nanoparticles yields $(Ni,Cu)_2P$ alloy but also unexpected outward migration of copper outside the nanoparticles.

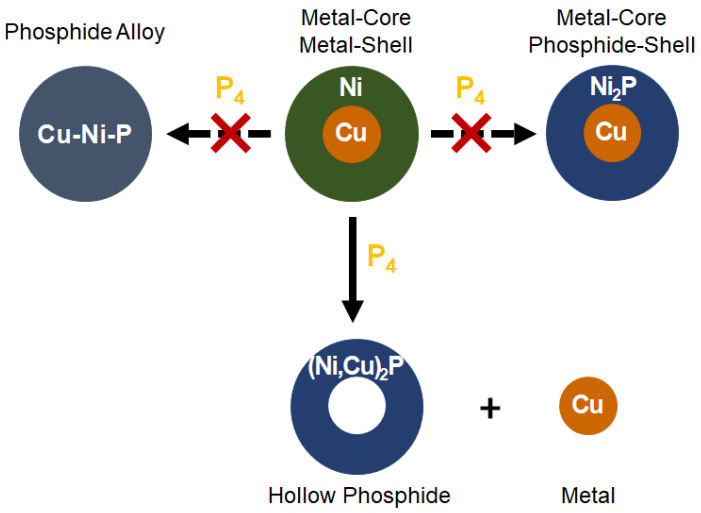

References

(1) Prins, R.; Bussell, M. E. Metal Phosphides: Preparation, Characterization and Catalytic Reactivity. *Catal. Letters* **2012**, *142* (12), 1413–1436.

(2) Oyama, S. T. Novel Catalysts for Advanced Hydroprocessing: Transition Metal Phosphides. *J. Catal.* **2003**, *216* (1–2), 343–352.

(3) Shi, Y.; Zhang, B. Recent Advances in Transition Metal Phosphide Nanomaterials: Synthesis and Applications in Hydrogen Evolution Reaction. *Chem. Soc. Rev.* **2016**, *45* (6), 1529–1541.

(4) Gregg, K. A.; Perera, S. C.; Lawes, G.; Shinozaki, S.; Brock, S. L. Controlled Synthesis of MnP Nanorods: Effect of Shape Anisotropy on Magnetization. *Chem. Mater.* **2006**, *18* (4), 879–886.

(5) Imai, M.; Michioka, C.; Ueda, H.; Yoshimura, K. Static and Dynamical Magnetic Properties of the Itinerant Ferromagnet LaCo2P2. *Phys. Rev. B* **2015**, *91* (18), 184414.

(6) Balli, M.; Fruchart, D.; Gignoux, D.; Tobola, J.; Hlil, E. K.; Wolfers, P.; Zach, R. Magnetocaloric Effect in Ternary Metal Phosphides (Fe1-XNix)2P. *J. Magn. Magn. Mater.* **2007**, *316* (2 SPEC. ISS.), 358–360.

(7) Gillot, F.; Boyanov, S.; Dupont, L.; Doublet, M. L.; Morcrette, M.; Monconduit, L.; Tarascon, J. M. Electrochemical Reactivity and Design of NiP2 Negative Electrodes for Secondary Li-Ion Batteries. *Chem. Mater.* **2005**, *17* (25), 6327–6337.

(8) Boyanov, S.; Annou, K.; Villevieille, C.; Pelosi, M.; Zitoun, D.; Monconduit, L.

Nanostructured Transition Metal Phosphide as Negative Electrode for Lithium-Ion Batteries. *Ionics (Kiel).* **2008**, *14* (3), 183–190.

(9) Boyanov, S.; Bernardi, J.; Bekaert, E.; Ménétrier, M.; Doublet, M. L.; Monconduit, L. P-Redox Mechanism at the Origin of the High Lithium Storage in NiP 2-Based Batteries. *Chem. Mater.* **2009**, *21* (2), 298–308.

(10) Micic, O. I.; Sprague, J. R.; Curtis, C. J.; Jones, K. M.; Machol, J. L.; Nozik, A. J.; Giessen, H.; Fluegel, B.; Mohs, G.; Peyghambarian, N. Synthesis and Characterization of InP, GaP, and GaInP2 Quantum Dots. *J. Phys. Chem.* **1995**, *99* (19), 7754–7759.

(11) Sharon, M.; Tamizhmani, G. Transition Metal Phosphide Semiconductors for Their Possible Use in Photoelectrochemical Cells and Solar Chargeable Battery (Saur Viddyut Kosh V). *J. Mater. Sci.* **1986**, *21* (6), 2193–2201.

(12) Wang, J.; Gudiksen, M. S.; Duan, X.; Cui, Y.; Lieber, C. M. Highly Polarized Photoluminescence and Photodetection from Single Indium Phosphide Nanowires. *Science (80-.).* **2001**, *293* (5534), 1455–1457.

(13) Mine, T.; Yanagi, H.; Kamiya, T.; Kamihara, Y.; Hirano, M.; Hosono, H. Nickel-Based Phosphide Superconductor with Infinite-Layer Structure, BaNi2P2. *Solid State Commun.* **2008**, *147* (3–4), 111–113.

(14) Popczun, E. J.; McKone, J. R.; Read, C. G.; Biacchi, A. J.; Wiltrout, A. M.; Lewis, N. S.; Schaak, R. E. Nanostructured Nickel Phosphide as an Electrocatalyst for the Hydrogen Evolution Reaction. *J. Am. Chem. Soc.* **2013**, *135* (25), 9267–9270.

(15) Tamang, S.; Lincheneau, C.; Hermans, Y.; Jeong, S.; Reiss, P. Chemistry of InP

Nanocrystal Syntheses. *Chem. Mater.* **2016**, *28* (8), 2491–2506.

(16) Henkes, A. E.; Schaak, R. E. Trioctylphosphine: A General Phosphorus Source for the Low-Temperature Conversion of Metals into Metal Phosphides. *Chem. Mater.* **2007**, *19* (17), 4234–4242.

(17) Carenco, S.; Hu, Y.; Florea, I.; Ersen, O.; Boissière, C.; Mézailles, N.; Sanchez, C. Metal-Dependent Interplay between Crystallization and Phosphorus Diffusion during the Synthesis of Metal Phosphide Nanoparticles. *Chem. Mater.* **2012**, *24* (21), 4134–4145.

(18) Mutinda, S. I.; Li, D.; Kay, J.; Brock, S. L. Synthesis and Characterization of Co2-XRhxP Nanoparticles and Their Catalytic Activity towards the Oxygen Evolution Reaction. *J. Mater. Chem. A* **2018**, *6* (25), 12142–12152.

(19) Li, D.; Baydoun, H.; Verani, C. N.; Brock, S. L. Efficient Water Oxidation Using CoMnP Nanoparticles. *J. Am. Chem. Soc.* **2016**, *138* (12), 4006–4009.

(20) Hitihami-Mudiyanselage, A.; Arachchige, M. P.; Seda, T.; Lawes, G.; Brock, S. L. Synthesis and Characterization of Discrete FexNi2-XP Nanocrystals ($0 < x < 2$): Compositional Effects on Magnetic Properties. *Chem. Mater.* **2015**, *27* (19), 6592–6600.

(21) Liyanage, D. R.; Danforth, S. J.; Liu, Y.; Bussell, M. E.; Brock, S. L. Simultaneous Control of Composition, Size, and Morphology in Discrete Ni2–XCoxP Nanoparticles. *Chem. Mater.* **2015**, *27* (12), 4349–4357.

(22) Liu, J.; Wang, Z.; David, J.; Llorca, J.; Li, J.; Yu, X.; Shavel, A.; Arbiol, J.; Meyns, M.; Cabot, A. Colloidal Ni2-: XCoxP Nanocrystals for the Hydrogen Evolution Reaction. *J. Mater. Chem. A* **2018**, *6* (24), 11453–11462.

(23) Henkes, A. E.; Schaak, R. E. Template-Assisted Synthesis of Shape-Controlled Rh2P Nanocrystals. *Inorg. Chem.* **2008**, *47* (2), 671–677.

(24) Duan, S.; Wang, R. Au/Ni12P5 Core/Shell Nanocrystals from Bimetallic Heterostructures: In Situ Synthesis, Evolution and Supercapacitor Properties. *NPG Asia Mater.* **2014**, *6* (9), e122–e122.

(25) Gilroy, K. D.; Ruditskiy, A.; Peng, H.-C.; Qin, D.; Xia, Y. Bimetallic Nanocrystals: Syntheses, Properties, and Applications. *Chem. Rev.* **2016**, *116* (18), 10414–10472.

(26) Yamauchi, T.; Tsukahara, Y.; Sakata, T.; Mori, H.; Yanagida, T.; Kawai, T.; Wada, Y. Magnetic Cu–Ni (Core–Shell) Nanoparticles in a One-Pot Reaction under Microwave Irradiation. *Nanoscale* **2010**, *2* (4), 515.

(27) Zhang, Y.; Huang, W.; Habas, S. E.; Kuhn, J. N.; Grass, M. E.; Yamada, Y.; Yang, P.; Somorjai, G. A. Near-Monodisperse Ni−Cu Bimetallic Nanocrystals of Variable Composition: Controlled Synthesis and Catalytic Activity for H 2 Generation. *J. Phys. Chem. C* **2008**, *112* (32), 12092–12095.

(28) Bonet, F.; Grugeon, S.; Dupont, L.; Herrera Urbina, R.; Guéry, C.; Tarascon, J. M. Synthesis and Characterization of Bimetallic Ni–Cu Particles. *J. Solid State Chem.* **2003**, *172* (1), 111–115.

(29) Liu, J.; Meyns, M.; Zhang, T.; Arbiol, J.; Cabot, A.; Shavel, A. Triphenyl Phosphite as the Phosphorus Source for the Scalable and Cost-Effective Production of Transition Metal Phosphides. *Chem. Mater.* **2018**, *30* (5), 1799–1807.

(30) Wang, R.; Dong, X. Y.; Du, J.; Zhao, J. Y.; Zang, S. Q. MOF-Derived

Bifunctional Cu3P Nanoparticles Coated by a N,P-Codoped Carbon Shell for Hydrogen Evolution and Oxygen Reduction. *Adv. Mater.* **2018**, *30* (6), 1703711.

(31) Peng, C. Y.; Kang, L.; Cao, S.; Chen, Y.; Lin, Z. S.; Fu, W. F. Nanostructured Ni2P as a Robust Catalyst for the Hydrolytic Dehydrogenation of Ammonia-Borane. *Angew. Chemie - Int. Ed.* **2015**, *54* (52), 15725–15729.

(32) Nowotny, H.; Henglein, E. Ein Beitrag Zur Kenntnis Ternärer Phosphorlegierungen. *Monatshefte für Chemie* **1948**, *79* (5), 385–393.

(33) Adlwarth, R.; Selke, H.; Ryder, P. L. Crystallization of Amorphous Cu-Ni-P Alloys. *Mater. Sci. Eng.* **1988**, *97*, 351–354.

(34) Zhao, M.; Ji, Y.; Wang, M.; Zhong, N.; Kang, Z.; Asao, N.; Jiang, W. J.; Chen, Q. Composition-Dependent Morphology of Bi-and Trimetallic Phosphides: Construction of Amorphous Pd-Cu-Ni-P Nanoparticles as a Selective and Versatile Catalyst. *ACS Appl. Mater. Interfaces* **2017**, *9* (40), 34804–34811.

(35) Kim, W.; Park, J. shin; Suh, C. yul; Ahn, J. G.; Lee, J. chun. Cu-Ni-P Alloy Nanoparticles Prepared by Electrical Wire Explosion. *J. Alloys Compd.* **2008**, *465* (1–2), L4–L6.

(36) Carenco, S.; Le Goff, X. F.; Shi, J.; Roiban, L.; Ersen, O.; Boissière, C.; Sanchez, C.; Mézailles, N. Magnetic Core-Shell Nanoparticles from Nanoscale-Induced Phase Segregation. *Chem. Mater.* **2011**, *23* (8), 2270–2277.

(37) Carenco, S.; Hu, Y.; Florea, I.; Ersen, O.; Boissière, C.; Sanchez, C.; Mézailles, N. Structural Transitions at the Nanoscale: The Example of Palladium Phosphides Synthesized from White Phosphorus. *Dalt. Trans.* **2013**, *42* (35), 12667.

(38) Carenco, S.; Demange, M.; Shi, J.; Boissière, C.; Sanchez, C.; Le Floch, P.; Mézailles, N. White Phosphorus and Metal Nanoparticles: A Versatile Route to Metal Phosphide Nanoparticles. *Chem. Commun.* **2010**, *46* (30), 5578.

(39) Carenco, S.; Boissière, C.; Nicole, L.; Sanchez, C.; Le Floch, P.; Mézailles, N. Controlled Design of Size-Tunable Monodisperse Nickel Nanoparticles. *Chem. Mater.* **2010**, *22* (4), 1340–1349.

(40) Frogneux, X.; Borondics, F.; Lefrançois, S.; D'Accriscio, F.; Sanchez, C.; Carenco, S. Surprisingly High Sensitivity of Copper Nanoparticles toward Coordinating Ligands: Consequences for the Hydride Reduction of Benzaldehyde. *Catal. Sci. Technol.* **2018**, *8* (19), 5073–5080.

(41) Liu, J.; Zheng, Y.; Hou, S. Facile Synthesis of Cu/Ni Alloy Nanospheres with Tunable Size and Elemental Ratio. *RSC Adv.* **2017**, *7* (60), 37823–37829.

(42) Carenco, S.; Labouille, S.; Bouchonnet, S.; Boissière, C.; Le Goff, X. F.; Sanchez, C.; Mézailles, N. Revisiting the Molecular Roots of a Ubiquitously Successful Synthesis: Nickel(0) Nanoparticles by Reduction of [Ni(Acetylacetonate) 2]. *Chem. - A Eur. J.* **2012**, *18* (44), 14165–14173.

(43) Nemoshalenko, V. V.; Didyk, V. V.; Krivitskii, V. P.; Senekevich, A. I. Investigation of the Atomic Charges in Iron, Cobalt and Nickel Phosphide. *Zh. Neorg. Khimii.* **1983**, *28*, 2182.

(44) Carenco, S.; Liu, Z.; Salmeron, M. The Birth of Nickel Phosphide Catalysts: Monitoring Phosphorus Insertion into Nickel. *ChemCatChem* **2017**, *9* (12), 2318–2323.

(45) Moreau, L. M.; Ha, D. H.; Zhang, H.; Hovden, R.; Muller, D. A.; Robinson, R.

D. Defining Crystalline/Amorphous Phases of Nanoparticles through X-Ray Absorption Spectroscopy and X-Ray Diffraction: The Case of Nickel Phosphide. *Chem. Mater.* **2013**, *25* (12), 2394–2403.

(46) Moreau, L. M.; Ha, D. H.; Bealing, C. R.; Zhang, H.; Hennig, R. G.; Robinson, R. D. Unintended Phosphorus Doping of Nickel Nanoparticles during Synthesis with TOP: A Discovery through Structural Analysis. *Nano Lett.* **2012**, *12* (9), 4530–4539.

(47) Yerushalmi, R.; Ho, J. C.; Fan, Z.; Javey, A. Phosphine Oxide Monolayers on SiO2 Surfaces. *Angew. Chemie* **2008**, *120* (23), 4512–4514.

(48) Carenco, S.; Wu, C. H.; Shavorskiy, A.; Alayoglu, S.; Somorjai, G. A.; Bluhm, H.; Salmeron, M. Synthesis and Structural Evolution of Nickel-Cobalt Nanoparticles under H2 and CO2. *Small* **2015**, *11* (25), 3045–3053.

(49) Franke, R.; Chassé, T.; Streubel, P.; Meisel, A. Auger Parameters and Relaxation Energies of Phosphorus in Solid Compounds. *J. Electron Spectros. Relat. Phenomena* **1991**, *56* (4), 381–388.

(50) Dera, P.; Lavina, B.; Borkowski, L. A.; Prakapenka, V. B.; Sutton, S. R.; Rivers, M. L.; Downs, R. T.; Boctor, N. Z.; Prewitt, C. T. Structure and Behavior of the Barringerite Ni End-Member, Ni2P, at Deep Earth Conditions and Implications for Natural Fe-Ni Phosphides in Planetary Cores. *J. Geophys. Res.* **2009**, *114* (B3), B03201.

(51) Chen, Y. C.; Chen, Z. B.; Lin, Y. G.; Hsu, Y. K. Synthesis of Copper Phosphide Nanotube Arrays as Electrodes for Asymmetric Supercapacitors. *ACS Sustain. Chem. Eng.* **2017**, *5* (5), 3863–3870.

(52) Nefedov, V. I.; Salyn, Y. V.; Domashevskaya, E. P.; Ugai, Y. A.; Terekhov, V. A. A Study by XPS and XRS of the Participation in Chemical Bonding of the 3d Electrons of Copper, Zinc and Gallium. *J. Electron Spectros. Relat. Phenomena* **1975**, *6* (3), 231–238.

(53) Biesinger, M. C.; Payne, B. P.; Lau, L. W. M.; Gerson, A.; Smart, R. S. C. X-Ray Photoelectron Spectroscopic Chemical State Quantification of Mixed Nickel Metal, Oxide and Hydroxide Systems. *Surf. Interface Anal.* **2009**, *41* (4), 324–332.

(54) Li, H.; Li, H.; Dai, W. L.; Wang, W.; Fang, Z.; Deng, J. F. XPS Studies on Surface Electronic Characteristics of Ni-B and Ni-P Amorphous Alloy and Its Correlation to Their Catalytic Properties. *Appl. Surf. Sci.* **1999**, *152* (1), 25–34.

(55) Blanchard, P. E. R.; Grosvenor, A. P.; Cavell, R. G.; Mar, A. X-Ray Photoelectron and Absorption Spectroscopy of Metal-Rich Phosphides M2P and M3P (M = Cr-Ni). *Chem. Mater.* **2008**, *20* (22), 7081–7088.

(56) Carenco, S. Designing Nanoparticles and Nanoalloys with Controlled Surface and Reactivity. *Chem. Rec.* **2018**, *18* (7), 1114–1124.

(57) Schlesinger, M. E. The Thermodynamic Properties of Phosphorus and Solid Binary Phosphides. *Chem. Rev.* **2002**, *102* (11), 4267–4302.

(58) Varón, M.; Ojea-Jimenez, I.; Arbiol, J.; Balcells, L.; Martínez, B.; Puntes, V. F. Spontaneous Formation of Hollow Cobalt Oxide Nanoparticles by the Kirkendall Effect at Room Temperature at the Water-Air Interface. *Nanoscale* **2013**, *5* (6), 2429–2436.

(59) Cabot, A.; Smith, R. K.; Yin, Y.; Zheng, H.; Reinhard, B. M.; Liu, H.; Alivisatos,

A. P. Sulfidation of Cadmium at the Nanoscale. *ACS Nano* **2008**, *2* (7), 1452–1458.

(60) Carenco, S.; Portehault, D.; Boissière, C.; Mézailles, N.; Sanchez, C. 25th Anniversary Article: Exploring Nanoscaled Matter from Speciation to Phase Diagrams: Metal Phosphide Nanoparticles as a Case of Study. *Adv. Mater.* **2014**, *26* (3), 371–389.

(61) Smigelskas, A. D.; Kirkendall, E. O. Zinc Diffusion in Alpha Brass. *Trans. AIME* **1947**, *171*, 130–142.

(62) Porter, D. A.; Easterling, K. E. *Phase Transformations in Metals and Alloys*; 1992.

(63) Nelson, A.; Ha, D. H.; Robinson, R. D. Selective Etching of Copper Sulfide Nanoparticles and Heterostructures through Sulfur Abstraction: Phase Transformations and Optical Properties. *Chem. Mater.* **2016**, *28* (23), 8530–8541.

(64) Allard, L. F.; Overbury, S. H.; Bigelow, W. C.; Katz, M. B.; Nackashi, D. P.; Damiano, J. Novel MEMS-Based Gas-Cell/Heating Specimen Holder Provides Advanced Imaging Capabilities for In Situ Reaction Studies. *Microsc. Microanal.* **2012**, *18* (04), 656–666.